Rare Metal Materials and Engineering
Volume 50, Issue 5, May 2021
Available online at www.rmme.ac.cn

Science Press

Cite this article as: Cheng Gong, Xiong Yuqing, Zhou Hui, et al. First-Principles Study on Adhesion, Stability, and Electronic Structure of Ir/SiC Interfaces[J]. Rare Metal Materials and Engineering, 2021, 50(05): 1569-1575.

ARTICLE

First-Principles Study on Adhesion, Stability, and Electronic Structure of Ir/SiC Interfaces

Cheng Gong, Xiong Yuqing, Zhou Hui, Zhang Kaifeng, Gao Hengjiao

Science and Technology on Vacuum Technology and Physics Laboratory, Lanzhou Institute of Physics, Lanzhou 730000, China

Abstract: The Ir(111)/SiC(111) interfaces were investigated by first-principles study based on density functional theory (DFT). Considering different stacking sites and terminations, six different interfaces were studied. The results show that an Ir(111) slab with 9 atom layers exhibits bulk-like interior characteristic, while a 12-atom-layer SiC(111) slab represents the properties of bulk SiC. Adhesion and interfacial energy results show that the C-terminated top-site (C-TS) and Si-terminated center-site (Si-CS) interfaces are highly stable with the highest work of adhesion of 6.35 and 6.23 J/m^2, and the smallest interfacial energy of 0.07 and 0.10 J/m^2 after relaxation, respectively. Electronic structure analysis reveals that the C-TS interface has the ionic characteristics, while the Si-CS interface exhibits covalent bond characteristics. The bonding strength and stability of C-TS and Si-CS interfaces are attributed to the hybridization between Ir-d and C-p, Si-p orbits. Compared with the C-TS interface, sub-interfacial atoms have more interaction with Ir atoms in Si-CS interface.

Key words: first-principles; Ir/SiC interface; work of adhesion; interfacial energy; electronic structure

High temperature materials have a wide range of applications in the aerospace, energy and national defense industries. At present, the commonly applied high temperature materials in aerospace mainly include refractory metals, super alloys and C/C composite materials. These materials have their own advantages, but the common disadvantage of these materials is that they are unable to maintain the performance for a long time in high-temperature oxidized environments. Anti-oxidation coating is probably the most effectively protective measure. Metal iridium (Ir) exhibits the unique physical and mechanical properties, such as high melting temperature (2430 ℃), excellent chemical compatibility, oxidation resistance, low oxygen and carbon permeability, which makes it a promising anti-oxidation coating candidate[1,2]. Normally, Ir coating can be prepared by many ways, such as chemical vapor deposition (CVD) [3,4], double-glow plasma deposition (DPD)[5,6] and molten salt electrodeposition (ED)[7,8]. However, the microstructures of Ir coatings prepared by these methods have a problem: the grain boundary of Ir coatings is normally perpendicular to the surface of the matrix, and the grain boundary can easily become the channel of oxidant penetration, resulting in coating failure[9-14]. Therefore, improving the microstructure of Ir coating is important for its application in a high-temperature and severe oxidizing environment.

Silicon carbide (SiC) is often used as reinforcement for various materials to improve the microstructure and properties of base material due to its distinct properties and good compatibility with other materials[15,16]. Abdollahi et al[17] studied the formation mechanism and erosion behavior of SiC-SiC_{nano} single-layer oxidation protective coating, and the results indicated that the density and adhesion of the coating increase with the addition of SiC nanoparticles, and the corrosion resistance significantly improves. Liu et al[18] studied the Al_2O_3 coatings doped with SiC particles and found that the surface roughness and friction coefficient of the coating decrease with the addition of SiC particles. Besides, SiC particles can change the electrical properties of the coating during deposition, reduce the plasma bombardment, and improve the structure of the coating. Bakhit[19] studied the effect of SiC on the performance of Ni and Ni-Co alloy coatings with addition of SiC nanoparticles and found significant changes in crystallite size and orientation. Thus, an Ir/SiC composite structure for improving the properties of Ir coating was proposed. Numerous research results indicated that the interface characteristics between SiC

Received date: May 19, 2020
Corresponding author: Xiong Yuqing, Ph. D., Professor, Science and Technology on Vacuum Technology and Physics Laboratory, Lanzhou Institute of Physics, Lanzhou 730000, P. R. China, Tel: 0086-931-4585987, E-mail: xiongyq@hotmail.com

and the matrix are critical for composites[20-24]. Therefore, a deeper investigation of interfacial structure of Ir/SiC is highly desirable.

First-principle calculations are widely employed to study the interfaces of atomic or even electronic scale for revealing the adhesion strength, stability and mechanism of interface bonding[25]. Xiong et al[26] simulated and analyzed the SiC/ZrB_2 composite coating and its electronic characteristics of the structure, and revealed that the structure is the most stable according to cohesive and interfacial energy. Jin et al[27] studied β-SiC(111)/α-W(110) interfaces in consideration of different terminations and stacking sites, and because the Si-terminated top-site interface is relatively stable from the view of electronic structure, the most stable configurations were confirmed by comparing the values of adhesion energy and interface energy. Li et al[28] simulated six different SiC/Ti interfaces and determined the most stable structure according to bonding strength and interface energy, and then pointed out that the hollow-sited structure has the largest fracture toughness and is prone to interface alloying to form new phases. The contribution of each orbital electron to the bonding was also analyzed. However, little research investigated the Ir/SiC interface through the first principle. Thus, the aim of this research is to systemically illustrate the adhesion strength, interfacial energy, electronic structure and bonding mechanism of the Ir/SiC system through first-principle calculations.

This research is structured as follows: (1) introduction of the calculation method and related parameters; (2) calculation of the properties of bulk Ir and SiC and the comparison between the calculated results and the reported results in the literature to certify the accuracy of the used calculation method. The appropriate number of atomic layers in Ir(111) and SiC (111) slabs was determined, and the properties of the Ir/SiC interface were investigated, such as work of adhesion, interfacial stability, electronic structure and bonding characteristics.

1 Computational Method

First-principle study was accomplished in the Cambridge Serial Total Energy Package (CASTEP) based on density functional theory[29]. The interaction between ions and valence electrons was described by plane-wave ultrasoft pseudopotential[30]. The valence electrons were Si $3s^23p^2$, C $2s^22p^2$ and Ir $5s^25p^65d^76s^2$. Generalized gradient approximation (GGA) with the Perdew-Burke-Ernzerhof (PBE) function was selected as exchange correlation function[31]. The cut-off energy was set as 400 eV. The 10×10×10 and 7×7×7 k-points were employed for Ir and SiC bulks, respectively, based on the convergence test results. The k-point for the following slabs and interfaces calculation was 10×10×1.

Kohn-Sham equation was solved with a self-consistent field (SCF) procedure to obtain the ground state[32]. The SCF convergence threshold was set as 1.0×10^{-6} eV/atom. Meanwhile, the geometry optimization was employed through Broyden-Fletcher-Goldfarb-Shanno (BFGS) algorithm to guarantee the minimum total energy of the system[33]. The convergence tolerance was 1.0×10^{-5} eV/atom for energy and 0.3 eV/nm for the maximum force.

2 Results and Discussion of Properties and Calculations About Bulk and Surface

2.1 Bulk properties

Both metal iridium and β-SiC belong to the typically face centered cubic (fcc) crystal structure with space group of Fm-3m and F-43m, respectively. To evaluate the reliability of the methodology, the parameters of bulk Ir and β-SiC were calculated before the model construction, and our calculated lattice constant (a), bulk modulus (B), elastic constant (C_{ij}) were compared with the published data, as listed in Table 1.

As shown in Table 1, for β-SiC, our calculated a and B are in good agreement with the published values[28,35]. Notably, the calculated lattice constant of β-SiC is larger than the value in Ref. [34], which is mainly due to the LDA over-bonding effect[38]. For Ir, our calculated parameters are also consistent with the published values[36,37]. Therefore, the calculation method adopted in this research can ensure the reliability of the following calculations.

2.2 Surface convergence and surface energy

Both Ir(111) and SiC(111) planes have considerable stability[39,40]. The Ir(111) and SiC(111) slabs were obtained by cutting Ir and β-SiC bulk and adding periodic boundary condition, as shown in Fig.1. An 1.5 nm vacuum layer was added to eliminate the interaction between the upper and lower free surfaces. SiC(111) plane is a typical polar surface with C-termination or Si-termination, as shown in Fig.1b and 1c, respectively.

To reduce the calculation time and ensure the accuracy, an appropriate number of atom layers for Ir(111) and SiC(111) slabs should be determined. The thickness of the slab can be confirmed by evaluating the variation of interlayer distances with increasing the number of atomic layers in slabs after relaxation. The variation of interlayer distance can be described as follows[41]:

$$\Delta_{ij} = \frac{d_{ij} - d_{ij}^0}{d_{ij}^0} \times 100\% \quad (1)$$

where d_{ij}^0 and d_{ij} are the atomic spacing between the adjacent i

Table 1 Calculated, theoretical and experimental lattice constant (a), bulk modulus (B) and elastic constant (C_{ij}) of bulk Ir and SiC

Material	Method	a/nm	B/GPa	C_{11}/GPa	C_{12}/GPa	C_{44}/GPa
β-SiC	GGA-PBE	0.4371	210.94	384.11	124.35	264.40
	GGA-PBE[28]	0.4363	211.61	385.00	124.92	241.63
	LDA[34]	0.4145	219	390	134	253
	Experiment[35]	0.4359	211	352	142	256
Ir	GGA-PBE	0.3869	346.47	591.70	223.86	252.30
	GGA-PW91[36]	0.388	343	-	-	-
	Experiment[37]	0.384	355	-	-	-

Note: LDA: local density approximation; GGA-PW91: generalized gradient approximation Perdew-Wang 91

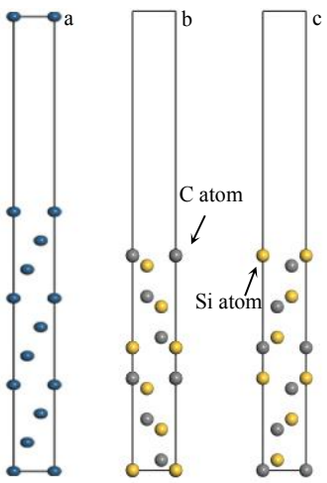

Fig.1 Surface structures of Ir(111) and SiC(111) plans: (a) 10-atom-layer Ir(111) slab; (b) C-terminated 12-atom-layer SiC(111) slab; (c) Si-terminated 12-atom-layer SiC(111) slab

and *j* interlayers before and after relaxation, respectively; $\Delta_{i/j}$ is the percentage of increase or decrease of interlayer distance after relaxation.

The alteration of interlayer spacing of SiC(111) and Ir(111) slabs changes as a function of termination and number of atom layers, as listed in Table 2. For polar SiC(111) plane, an odd-atom-layer slab with the same atom type at two ends should be adopted to avoid the dipole effect because the terminal surface of SiC(111) contains only one kind of atoms (Si or C). However, an odd number of layers results in nonstoichiometric Si and C atoms. Furthermore, each surface atom of the slab has three unsaturated bonds, which is less thermodynamically favorable according to the thermodynamics theory. Therefore, an even-number atom layer SiC(111) slab was adopted. It can be seen from Table 2 that the variation of interlayer distance in the SiC(111) slab is mainly concentrated in the three outmost layers, the first interlayer distance of all slabs shrinks, and the change of the interlayer spacing from the outside to the inside is in a contraction/expansion cycle. Compared with the interlayer spacing of Si-terminated surface, the outmost interlayer spacing of C-terminated SiC(111) surface changes more obviously, which indicates that the C-terminated SiC(111) surface has a higher activity than that of Si-terminated surface. With increasing the number of atomic layers, the variation of interlayer distance decreases gradually. The change in the interlayer spacing of the slabs is already very small when the number of atomic layers, $N \geqslant 10$. Compared with the SiC(111) slab, the main variation of the atomic spacing in the Ir(111) slabs is concentrated in $\Delta_{1/2}$. As shown in Table 2, the inner interlayer spacing of the Ir(111) slabs hardly changes after relaxation when the number of atomic layers$\geqslant$8. Therefore, a 12-atom-layer SiC(111) and a 10-atom-layer Ir (111) slab are sufficient to show the bulk-like interiors and guarantee the accuracy of calculation results.

Surface energy (γ_s) is defined as the energy required to form

Table 2 Interlayer spacing variation of SiC(111) and Ir(111) slabs (%)

Material	Interlayer	Number of layers, *N*				
		6	8	10	12	14
SiC(111)	$\Delta_{1/2}$	−28.01	−20.7	−22.31	−22.34	−22.22
	$\Delta_{2/3}$	8.86	2.91	2.87	2.48	2.22
	$\Delta_{3/4}$	−22.22	−8.25	−5.54	−4.44	−3.81
	$\Delta_{4/5}$	12.04	3.06	1.69	1.11	0.89
	$\Delta_{5/6}$	−50.21	−11.57	−5.55	−3.65	−2.86
	$\Delta_{6/7}$	-	6.87	1.96	1.00	0.63
	$\Delta_{7/8}$	-	−43.26	−8.87	−3.65	−2.54
	$\Delta_{8/9}$	-	-	5.87	1.48	0.74
	$\Delta_{9/10}$	-	-	−42.38	−7.62	−2.86
	$\Delta_{10/11}$	-	-	-	5.71	1.27
	$\Delta_{11/12}$	-	-	-	−42.70	−7.46
	$\Delta_{12/13}$	-	-	-	-	5.60
	$\Delta_{13/14}$	-	-	-	-	−42.86
	Interlayer	Number of layers, *N*				
		5	6	7	8	9
Ir	$\Delta_{1/2}$	−3.55	−3.64	−3.77	−3.78	−3.64
	$\Delta_{2/3}$	−1.78	−1.64	−1.20	−1.18	−1.19
	$\Delta_{3/4}$	−1.78	−1.11	−1.02	−1.09	−1.15
	$\Delta_{4/5}$	−3.60	−1.60	−1.02	−1.04	−1.03
	$\Delta_{5/6}$	-	−3.68	−2.09	−1.09	−1.03
	$\Delta_{6/7}$	-	-	−3.68	−1.18	−1.51
	$\Delta_{7/8}$	-	-	-	−3.78	−2.00
	$\Delta_{8/9}$	-	-	-	-	−3.51

Note: positive and negative values of $\Delta_{i/j}$ indicate the expansion and contraction of the interlayer spacing, respectively; for material SiC(111), $\Delta_{1/2}$ indicates the Si termination, and $\Delta_{5/6}$, $\Delta_{7/8}$, $\Delta_{9/10}$, $\Delta_{11/12}$, and $\Delta_{13/14}$ indicate the C termination for slabs with different thicknesses

a new unit area of surface when the crystal is separated into two free surfaces along a specific plane and normally employed to describe the surface stability. The surface energy (γ_s) can be obtained by Eq.(2)[42]:

$$\gamma_s = \frac{E_{slab} - NE_{bulk}}{2A_s} \quad (2)$$

where E_{slab} represents the total energy of the slab, N is the total number of the primitive cells in the slab, E_{bulk} denotes the total energy of the primitive cells, A_s represents the surface area, and the factor 2 means that there are two surfaces.

The surface energies of Ir(111) and SiC(111) slabs with increasing the atomic layer are shown in Table 3. The surface energy of Ir(111) slabs decreases with increasing the number of atomic layer, and converges to a constant value of 2.04 J/m^2 when the number of atomic layers, $N \geqslant 10$, which demonstrates that the 10-atom-layer Ir(111) slab is sufficient to represent the properties of bulk Ir. It is also consistent with the abovementioned variation of interlayer spacing in the Ir(111) slab.

Since the atom types at the two ends of SiC slab are different, the calculated surface energy according to Eq.(2) is the av-

erage value of the surface energies of the C and Si terminations, i.e., $\gamma_{s\text{-}SiC(111)}=(\gamma_{s\text{-}C\text{-}SiC(111)}+\gamma_{s\text{-}Si\text{-}SiC(111)})/2$[27]. Table 3 shows that the surface energy of SiC(111) converges to 4.24 J/m^2 when the number of atom layers, $N\geqslant 12$. The number of atom layers determined by surface energy equals the number of atom layers confirmed by Eq.(1). Our calculated surface energy is also consistent with those published results of 4.16[26] and 4.33[27] J/m^2. It is further convinced that the selected atom layers in SiC(111) slab is reasonable.

Ir atoms can be located at three different positions of SiC(111) surface: top-site, center-site and hollow-site, as shown in Fig. 3. The top-site means that the interfacial Ir atoms are directly located on the top of C atoms in the first layer from SiC side (Fig.3a and 3d); the center-site denotes that the interfacial Ir atoms are placed on the top of Si atoms in the second layer from SiC side (Fig.3b and 3e); the hollow-site indicates that the interfacial Ir atoms are situated on the top of Si atoms in the fourth layer from SiC side (Fig.3c and 3f). The models in Fig.3a~3c are named as C-TS, C-CS and C-HS, respectively. Si-terminated situation is similar to that of C-terminated ones, i.e., the related modals are named as Si-TS, Si-CS, and Si-HS.

2.3 Model geometry

According to the test results, Ir(111)/SiC(111) interfaces are constructed by stacking 10-atom-layer Ir(111) on 12-atom-layer SiC(111). The orientation relationships are Ir(111)//SiC(111) and Ir[$1\bar{2}1$]//SiC[$1\bar{2}1$]. The lattice constant of (1×1)Ir(111) and (1×1)SiC(111) slabs is 0.282 427 2 and 0.310 186 5 nm, respectively. The Ir(111)/SiC(111) interface is a coherent interface with a lattice misfit of 4.68%. A vacuum layer of 1.5 nm was added to prevent the interaction between the upper and lower free surface, as shown in Fig.2.

2.4 Work of adhesion

Interface bonding strength can be evaluated by the work of adhesion (W_{ad}), which is mainly originated from the electronic interaction of atoms at the interface. A large W_{ad} suggests a high bonding strength. W_{ad} can be expressed as follows[43]:

$$W_{ad}=\frac{E_{Ir}^{total}+E_{SiC}^{total}-E_{Ir/SiC}^{total}}{A} \quad (3)$$

where E_{Ir}^{total} represents the total energy of the isolated 10-atom-layer Ir(111) slab, E_{SiC}^{total} indicates the total energy of the isolated 12-atom-layer SiC(111) slab, $E_{Ir/SiC}^{total}$ is the total energy of the Ir/SiC system, and A is the interfacial area.

W_{ad} can be calculated by unrelaxed geometries and relaxed geometries. By the former one, the total energy of unrelaxed models with different distances d_0 (0.08~0.34 nm) is calculated, and then the relationship of W_{ad} and interface distance d_0 is obtained, as shown in Fig.4. The work of adhesive of six interface structures increase first and then decrease with the in-

Table 3 Surface energy (γ_s) of Ir(111) and SiC(111) slabs with different numbers of layers

Number of layers, N	Surface energy, γ_s/J·m^{-2}	
	Ir(111)	SiC(111)
6	2.20	3.94
7	2.13	-
8	2.09	4.14
9	2.06	-
10	2.04	4.21
11	2.04	-
12	-	4.24
14	-	4.24
16	-	4.24

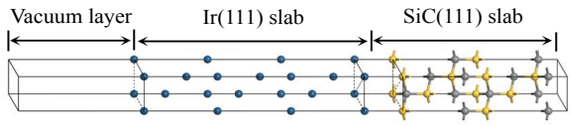

Fig.2 Schematic diagram of Ir/SiC interface (blue spheres are Ir atoms, grey spheres are C atoms and yellow spheres are Si atoms)

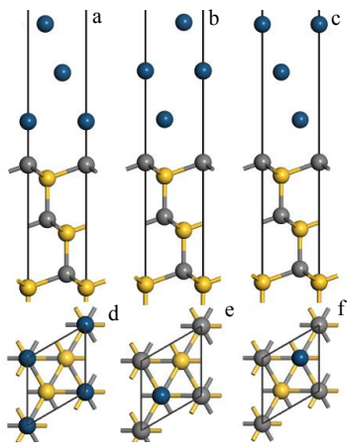

Fig.3 Cross (a~c) and top (d~f) views of three stacking sites of the C-terminated Ir(111)/SiC(111) interfaces: (a, d) top-site, (b, e) center-site, and (c, f) hollow-site

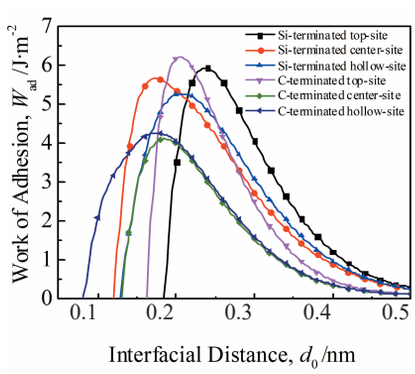

Fig.4 Relationship between W_{ad} and interface distance d_0 for six different Ir/SiC interface models

crease of interface distance. The maximum W_{ad} corresponds to the optimal interfacial distance d_0, which is 0.24 nm for Si-TS, 0.18 nm for Si-CS, C-CS and C-HS, and 0.20 nm for Si-HS and C-TS. In another case, the optimal interfacial separation is used to build the interfacial model, and then the total energy of these six structures at equilibrium state is obtained after full relaxation. The optimal d_0 and W_{ad} values for relaxed geometries are shown in Table 4.

It can be seen from Table 4 that both the termination and stacking site influence W_{ad}. Compared with unrelaxed structures, the interface distance d_0 of six structures decreases after relaxation, the reduced interface distance implies stronger interaction of atoms at the interface, which can be verified from the increased W_{ad} after relaxation. For the C-terminated interface, the C-TS stacking structure has the largest W_{ad} (6.35 J/m^2) followed by the C-HS structure, and the C-CS interface is the least favorable structure due to its smallest W_{ad} (4.45 J/m^2). Thus, Ir atoms prefer to locate on the top of C atoms in the first layer of SiC(111) surface. As for the Si-terminated ones, the Si-CS structure has the largest W_{ad} (6.23 J/m^2), indicating that the bonding strength of the Si-CS interface is greater than that of the other two interfaces. Among these six interface structures, the C-TS and Si-CS interfaces are the most stable structures with the largest W_{ad}.

2.5 Interfacial energy

Interfacial energy (γ_{int}) is another important factor to quantitatively analyze the interface stability. Interfacial energy is difficult to measure experimentally because it is essentially derived from the interfacial atomic chemical bonds and strain when different materials are combined, which can be described by Eq.(4)[44]:

$$\gamma_{int} = \frac{E_{Ir/SiC}(N,M) - NE_{Ir}^{bulk} - ME_{SiC}^{bulk}}{A} - \gamma_{Ir} - \gamma_{SiC} \quad (4)$$

where $E_{Ir/SiC}$ is the total energy of the Ir/SiC interface at equilibrium distance; E_{Ir}^{bulk} and E_{SiC}^{bulk} are the total energy of primitive Ir and SiC cells, respectively; N and M represent the number of Ir atoms and SiC compounds in the interface, respectively; γ_{Ir} and γ_{SiC} are the calculated surface energies of the Ir and SiC slabs, respectively; A is the area of the interface.

Generally, a stable interface structure has a small interfacial energy. The calculated interfacial energies of the six models are shown in Table 5. It is clear that the C-TS and Si-CS interfaces exhibit the lowest interfacial energy of 0.07 and 0.10 J/m^2, respectively, indicating that these two models are the most stable structures, which is consistent with the calculated W_{ad}.

Table 4 Work of adhesion (W_{ad}) and interfacial distance (d_0) for unrelaxed and relaxed Ir/SiC interface structures

Termination	Stacking	Unrelaxed		Relaxed	
		d_0/nm	W_{ad}/J·m^{-2}	d_0/nm	W_{ad}/J·m^{-2}
C	TS	0.20	5.74	0.1964	6.35
	CS	0.18	4.01	0.1743	4.55
	HS	0.18	3.97	0.1782	4.68
Si	TS	0.24	5.40	0.2383	5.72
	CS	0.18	5.51	0.1784	6.23
	HS	0.20	5.08	0.1921	6.07

Table 5 Interfacial energy (γ_{int}) of six different interfaces (J·m^{-2})

Model	Stacking position	γ_{int}
C-terminated	Top-site	0.07
	Centre-site	2.13
	Hollow-site	1.79
Si-terminated	Top-site	0.15
	Centre-site	0.10
	Hollow-site	0.55

2.6 Electronic structure

The interface strength and stability of the Ir/SiC are related to the interfacial electronic structure. Thus, the charge density differences of the Ir(111)/SiC(111) interfaces were analyzed. The C-TS and Si-CS interfaces are the most stable structures with the highest W_{ad} and lowest γ_{int}, so the electronic structure analyses focus on these two structures. The charge density differences of the C-TS and Si-CS structures are presented in Fig. 5. The blue color indicates electrons losing, and the red color means the electrons accumulating. The charge redistribution of the two structures is concentrated near the interface. For the C-TS interface (Fig.5a), the transferred charge from interfacial Ir atoms accumulates towards the SiC side. It can be speculated that the Ir-C bonds form at the C-TS interface with ionic bond characteristics. For the Si-CS interface (Fig. 5b), the accumulated charge at the interface region is shared by interfacial Ir and Si atoms. The shared charge comes from Ir atoms of the Ir(111) side and Si atoms of the SiC(111) side, indicating that Ir-Si bonds form cross the interface with covalent bond characteristics. Compared with the Si-CS interface, the charge accumulation at the interface of the C-TS structure is significantly stronger, because C-TS interface has a larger W_{ad}.

To further study the bonding characteristics of the C-TS and Si-CS interfaces, the partial density of states (PDOS) of the C-TS and Si-TS interfaces were investigated and presented in Fig.6, in which the dotted line denotes the Fermi level. The total density of states (TDOS) curves of C-TS and Si-TS inter-

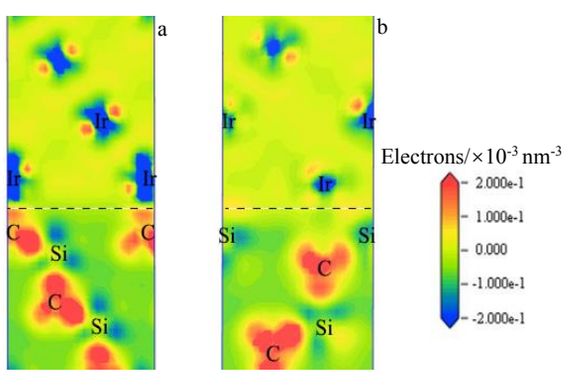

Fig.5 Charge density differences for relaxed Si-TS (a) and C-TS (b) interfaces (the dotted line indicates the interface)

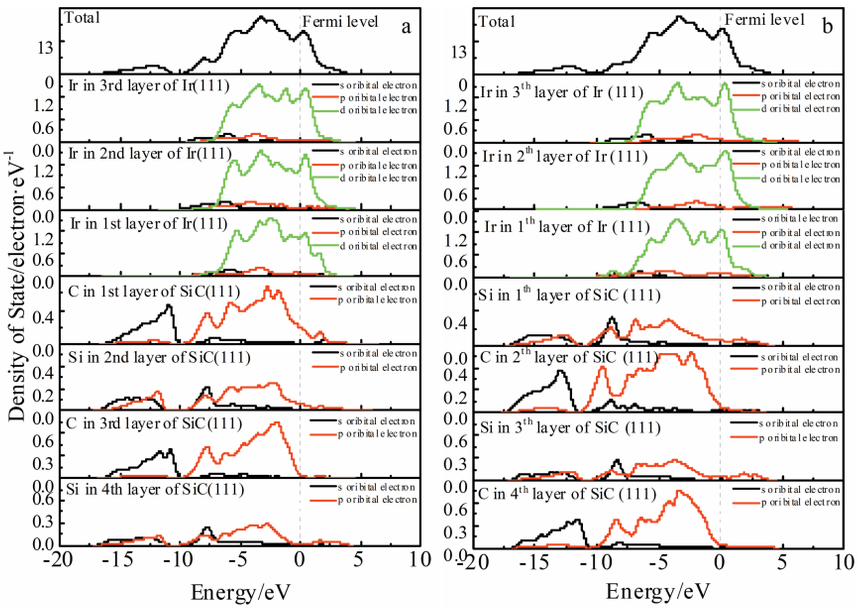

Fig.6 Partial density of states (PDOS) for C-TS interface (a) and Si-CS interface (b)

faces are similar throughout the energy range, indicating that these two interfaces have similar electronic structures. Meanwhile, the two distinct peaks are observed near the Fermi level, indicating that both the interfaces have metallic features. The density of states (DOS) values of the C-TS and Si-CS interfaces near the Fermi level are 16.33 and 17.77 electron/eV, respectively. The larger value of 17.77 electron/eV means that the Si-CS interface has stronger metallic behavior than C-TS structure does.

For the C-TS interface (Fig.6a), the TDOS shows a low energy state appearing between −17 and −11 eV, which is mainly contributed by C-s and Si-sp orbits, while the TDOS peaks in the range from −10 eV to 0 eV are attributed to the Ir-d, C-p and Si-p orbits. For interfacial atoms, the Ir-d and C-p overlapping states can be observed between −7.5 and −2.5 eV, and a new state appears for both the Ir-d and C-p orbits at 1 eV. These results indicate that the adhesion and stability of C-TS interface is mainly due to the interaction of Ir-d and C-p orbits. For the Si-CS interface (Fig.6b), the low energy state is mainly due to C-s and Si-sp, which is similar to the situation of C-TS interface. The TDOS peaks in the range from −10 eV to 0 eV are mainly attributed to the Ir-d, C-p and Si-p orbits. Compared with the C-TS interface, sub-interfacial atoms of the SiC side contribute much more than interface atoms does. The interfacial Ir-d orbit has more overlapping states with sub-interface C-p. The Ir-C bonds form, therefore, the interface adhesion and stability mainly result from the interaction of Ir-d, Si-p and C-p orbits.

3 Conclusions

1) A 10-atom-layer Ir(111) slab is sufficient to represent the properties of the bulk Ir, while a SiC(111) slab with 12 layers possesses the bulk-like interior.

2) Electron structure analysis shows that the charge of interfacial Ir atoms transfers to the SiC side in C-terminated top-site (C-TS) interface, showing the ionic characteristics. While the charge from Ir, Si and C accumulates at the interface region and exhibits covalent bond characteristics in Si-terminated center-site (Si-CS) interface. Compared with the Si-CS interface, the charge accumulation at the interface of the C-TS structure is more obvious.

3) The partial density of states shows that the total density of states mainly results from the Ir-d, C-p and Si-p orbits; the C-TS interface mainly consists of Ir-C bonds, while the Ir-Si and Ir-C bonds form in the Si-CS interface. Compared with the C-TS interface, sub-interfacial atoms have more interactions with Ir atoms in Si-CS interface.

References

1 Halvorson J J, Wimber R T. *Journal of Applied Physics*[J], 1972, 43(6): 2519

2 Mumtaz K, Echigoya J, Enoki H *et al*. *Journal of Materials Science*[J], 1995, 30: 465

3 Vargas G J R, Goto T. *Materials Transactions*[J], 2003, 44(9): 1717

4 Maury F, Senocq F. *Surface and Coatings Technology*[J], 2003, 163-164: 208

5 Wang Liangbing, Chen Zhaofeng, Zhang Ying *et al*. *International Journal of Refractory Metals and Hard Materials*[J], 2009, 27(3): 590

6 Wu Wangping, Lin Xin, Chen Zhaofeng *et al*. *Plasma Chemistry and Plasma Processing*[J], 2011, 31(3): 465

7 Zhu Li'an, Bai Shuxin, Zhang Hong. *Surface and Coatings Technology*[J], 2011, 206(6): 1351

8 Zhu Li'an, Bai Shuxin, Zhang Hong *et al*. *Applied Surface Sci-*

ence[J], 2013, 265: 537
9 Fortini A, Tuffias R. *35th Joint Propulsion Conference and Exhibit*[C]. Los Angeles: American Institute of Aeronautics & Astronautics, 1999: 2894
10 Hamilton J C, Yang N Y C, Clift W M *et al*. *Metallurgical Transactions A*[J], 1992, 23(3): 851
11 Bai Shuxin, Zhu Li'an, Zhang Hong *et al*. *International Journal of Refractory Metals and Hard Materials*[J], 2013, 41: 563
12 Wu Wangping, Chen Zhaofeng, Wang Liangbing. *Protection of Metals and Physical Chemistry of Surfaces*[J], 2015, 51(4): 607
13 Chen Zhaofeng, Wu Wangping, Cong Xiangna *et al*. *Advanced Manufacturing Technology*[J], 2011, 314-316: 214
14 Huang Yongle, Bai Shuxin, Zhang Hong *et al*. *Surface & Coatings Technology*[J], 2016, 288: 52
15 Luo X, Yang Y Q, Liu Y C *et al*. *Materials Science and Engineering A*[J], 2007, 459(1-2): 244
16 Das M, Balla V K, Basu D *et al*. *Scripta Materialia*[J], 2010, 63(4): 438
17 Abdollahi A, Torabi S, Valefi Z *et al*. *Corrosion Science*[J], 2019, 159: 108 136
18 Liu Chenxu, Zhang Shuguang, Ruonan Ji *et al*. *Ceramics International*[J], 2019, 45(4): 4747
19 Bakhit B, Akbari A. *Surface and Coatings Technology*[J], 2014, 253: 76
20 Cho S, Jo I, Y Lee H *et al*. *Applied Surface Science*[J], 2018, 448: 407
21 Tanaka Y, Kagawa Y, Liu Y F *et al*. *Materials Science and Engineering A*[J], 2001, 314(1-2): 110
22 Franco M, Sha W, Tan V *et al*. *Materials & Design*[J], 2015, 85: 248
23 Mandal D, Viswanathan S. *Materials Characterization*[J], 2013, 85: 73
24 Yang Y, Cheng Y F. *Electrochimica Acta*[J], 2013, 109: 638
25 Finnis M W, Kruse C, Schönberger U. *Nanostructured Materials*[J], 1995, 6(1-4): 145
26 Xiong Huihui, Liu Zhao, Zhang Henghua *et al*. *Journal of Physics and Chemistry of Solids*[J], 2017, 107: 162
27 Jin Na, Yang Yanqing, Luo Xian *et al*. *Applied Surface Science*[J], 2014, 314: 896
28 Li Jian, Yang Yanqing, Li Lili *et al*. *Journal of Applied Physics*[J], 2013, 113(2): 23 516
29 Vanderbilt D. *Physical Review B*[J], 1990, 41(11): 7892
30 Segall M D, Lindan P J D, Probert M J *et al*. *Journal of Physics, Condensed Matter*[J], 2002, 14(11): 2717
31 White J A, Bird D M. *Physical Review B*[J], 1994, 50(7): 4954
32 Kohn W, Sham L J. *Physical Review*[J], 1965, 140(4A): 1133
33 Fischer T H, Almlof J. *The Journal of Physical Chemistry*[J], 1992, 96(2): 9768
34 Karch K, Pavone P, Windl W *et al*. *International Journal of Quantum Chemistry*[J], 1995, 56(6): 801
35 Madelung O, Rössler U, Schulz M. *Silicon Carbide*[M]. Heidelberg: Springer, 2001
36 Gong H R, Liu Y, Tang H P *et al*. *Applied Physics Letters*[J], 2008, 92(21): 211 914
37 Yamabe-Mitarai Y, Koizumi Y, Murakami H *et al*. *Scripta Materialia*[J], 1997, 36(4): 393
38 Arbouche O, Belgoumène B, Soudini B *et al*. *Computational Materials Science*[J], 2010, 47(3): 685
39 Reznik B, Gerthsen D, Zhang W G *et al*. *Journal of the European Ceramic Society*[J], 2003, 23(9): 1499
40 Lee Y J, Choi D J, Park J Y *et al*. *Journal of Materials Science*[J], 2000, 35(18): 4519
41 Bi Kai, Liu Jun, Dai Qixun. *Applied Surface Science*[J], 2012, 258(10): 4581
42 Fiorentini V, Methfessel M. *Journal of Physics, Condensed Matter*[J], 1998, 10: 895
43 Siegel D G, Hector Jr L G, Adams J B. *Surface Science*[J], 2002, 498(3): 321
44 Pan Y, Lin Y H, Wang H *et al*. *Computational Materials Science*[J], 2016, 111: 74

Ir/SiC界面结合力、稳定性和电子结构的第一性原理研究

成　功，熊玉卿，周　晖，张凯锋，高恒蛟
(兰州空间技术物理研究所 真空科学技术物理实验室，甘肃 兰州 730000)

摘　要：基于密度泛函理论（DFT）第一性原理研究了Ir(111)/SiC(111)界面。在考虑不同堆垛位置和表面封端的基础上，共研究了6种不同的界面构型。结果表明：具有9层原子层的Ir(111)表面构型表现体相材料的特征，而12层原子层的SiC(111)表面构型能体现体相SiC的性能。粘附功和界面能结果表明，C封端顶位堆垛（C-TS）和Si封端中心位堆垛（Si-CS）界面构型具有最大的粘附功，分别为6.35和6.23 J/m^2，是最稳定的构型；弛豫后的界面能分别为0.07和0.10 J/m^2。电子结构分析表明：C-TS界面处具有离子特性，而Si-CS界面处具有共价键特性。C-TS和Si-CS界面的结合强度和稳定性归因于Ir-d与C-p，Si-p轨道之间的杂化。与C-TS界面相比，Si-CS界面第2层原子与界面Ir原子的相互作用更大。

关键词：第一性原理；Ir/SiC界面；粘附功；界面能；电子结构

作者简介：成　功，男，1988年生，博士生，兰州空间技术物理研究所，甘肃 兰州 730000，E-mail：gcheng@cqu.edu.cn